On the equilibrium limit of liquid stability in pressurized aqueous systems

Arian Zarriz[1], Baptiste Journaux[3^], Matthew J. Powell-Palm[1,2^]

[1]J. Mike Walker '66 Department of Mechanical Engineering, Texas A&M University, College Station, TX, USA

[2]Department of Materials Science & Engineering, Texas A&M University, College Station, TX, USA

[3]Department of Department of Earth and Space Sciences, University of Washington, Seattle, WA, USA

Correspondence:
BJ (bjournau@uw.edu)
MPP (powellpalm@tamu.edu)

Abstract:
Phase stability, and the limits thereof, are a central concern of materials thermodynamics. However, the temperature limits of equilibrium liquid stability in chemical systems have only been widely characterized under constant (typically atmospheric) pressure conditions, whereunder the limit is represented by the eutectic. At higher pressures, this limit will shift in both temperature and chemical composition, opening a wide thermodynamic parameter space over which the absolute limit, i.e., the limit under arbitrary values of the thermodynamic forces at play (here pressure and concentration), might exist. In this work, we use isochoric freezing to measure this absolute limit for the first time in several binary aqueous brines, and, nodding to the etymology of "eutectic", we name this limit the "cenotectic" (from Greek "κοινός-τῆξῐς", "universal-melt"). We observe that when no solute-bearing high-pressure phases exist, the cenotectic occurs consistently 22±2K below the 1 bar eutectic and at approximately 213±3 MPa, suggesting domination by the liquidus behaviors of the icy phases present. In charting the T-P evolution of each eutectic configuration, we also encounter several unreported high-pressure hydrates of $NaHCO_2$, $MgCl_2$, and $NaCl$, and we find that these high-pressure phases can produce complex multi-phase configurations involving the liquid that may remain metastable to significantly lower temperatures. We discuss the implications of these findings for ocean worlds of our solar system and cold ocean exoplanets; estimate thermodynamic limits on ice crust thickness and final ocean depth ("endgame") using the cenotectic pressure; and finally provide a generalized thermodynamic perspective on (and definition for) this fundamental thermodynamic invariant point.

Introduction:

Multiphase liquid-solid equilibrium ranks amongst the most fundamental concepts in thermodynamics and physical chemistry, providing the foundation of modern phase diagrams, grounding thermodynamic analysis, and driving countless industrial processes. In multicomponent systems, at constant pressure, the lowest temperature at which a liquid may remain stable at equilibrium is defined as the eutectic (from Greek εὐ-τῆξῐς, "easy-melt"), an invariant point in temperature-concentration (T-x) space at which the liquid will transition entirely into a mixture of solid phases. Eutectics are of crucial importance to a wide range of applications, from metallurgy to igneous rock formation, phase change thermal energy storage to cryopreservation, drug discovery to planetary science, and etc. The canonical definition of the eutectic is often considered at a fixed pressure (typically 1 atmosphere); however, increased states of compression may substantially affect the melting curves of solids, resulting in a change of eutectic T-X coordinates. When pressure is varied, the eutectic becomes a univariant line in the P-T-X space, the trajectory of which depends upon the geometry of the liquidus curves of the contributing solid phases.

For most materials, solid phases are denser than the liquid phase, meaning these materials possess positive Clapeyron melting slopes (dP/dT>0). For systems containing such solids, univariant eutectic line temperatures will increase with increasing pressures.

Select compounds in natural science and engineering however, such as water, silicon, or gallium, have negative Clapeyron melting slopes at 1 atmosphere (i.e., select solid phases of these compounds are less dense than the liquid). In many binary systems containing these compounds, initial compression from 1 atmosphere leads to pressure-induced melting point depression, resulting in the univariant eutectic line decreasing in temperature with increasing pressure(1). However, for all of these systems, continued compression of the liquid will eventually result in the formation of a denser solid phase (e.g. ice III, Si-II, Ga-II), thereby reversing the Clapeyron slope. In this context, the negative-Clapeyron eutectic line for the lower pressure range will intersect a positive-Clapeyron higher-pressure melting line at an invariant point in P-T-X space.
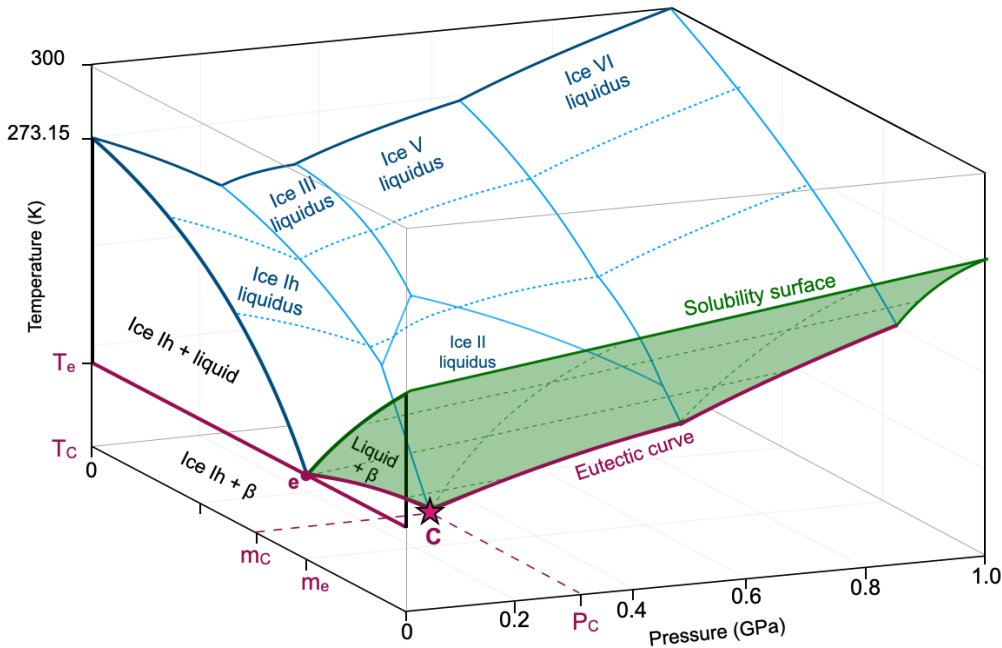
Figure 1: Conceptual pressure-temperature-concentration phase diagram for a binary solution of water and a generic salt-like solute, with the eutectic at ambient pressure marked (**e**), the pressure-dependent eutectic curve marked by the thick magenta line, and the cenotectic point (**C**) marked as a star.

For aqueous solutions in which the eutectic in equilibrium with ice-Ih is the lowest-temperature eutectic in the phase diagram (including most solutions of salts, sugars, and other solutes that are solid at room temperature), this invariant point represents the lowest possible temperature at which a given liquid phase may remain stable at equilibrium under *any* P-T-X conditions, and therefore represents a fundamental property of the system. Based on the etymology of eutectic (from Greek "εὐ-τῆξῐς" , "easy-melt"), we propose the name cenotectic (from Greek "κοινός-τῆξῐς", "universal-melt") for this invariant point, and we illustrate it in Figure 1, which presents a semi-quantitative P-T-X diagram for a binary system of water and a generic salt-like solute.

In this work, we describe first-of-their-kind experimental determinations of the precise P-T coordinates of the cenotectic points of major binary aqueous systems relevant to the planetary sciences, medical sciences, and engineering. These results are acquired via cryogenic-temperature extension of the isochoric freezing approach described in Chang et. al.(1), and are complemented by the discovery of several new high-pressure hydrate phases. While select previous works have inadvertently observed the cenotectic transition during the study of high-pressure univariant equilibria (2–4), to our knowledge, no previous research has indentified or measured the invariant point itself, nor defined it as an entity distinct from other univariant transitions. We will discuss the implications of this data on our evolving understanding of low-temperature aqueous thermodynamics, detail implications on the planetary science of icy worlds, and provide a suggested roadmap toward rapid illumination of the yet-unexplored low-temperature high-pressure parameter space for aqueous solutions. In closing, we will provide a generalized definition of the cenotectic, applicable to arbitrary chemical systems under the influence of any arbitrary modes of thermodynamic work.

Results:

We used isochoric freezing (1) to measure the pressure-temperature evolution of the eutectic for eight aqueous binary solutions (Na_2CO_3, KCl, $MgSO_4$, Na_2SO_4, Urea, NaCL, $MgCl_2$, and $NaHCO_3$) in the temperature range 273.15 to 203K and the pressure range 0.1 to 250 MPa, identifying the P-T coordinates of the cenotectic point in six of them and pointing at new possible high-pressure hydrate phases in the remaining three (NaCl, MgCl2, NaHCO3). The eutectic P-T curves for all eight solutions are shown in Fig. 2. Details on the isochoric freezing process are provided in the Methods and in Supplementary Note S1, with chamber schematics provided in Supplementary Figure S1. Additional discussion of the thermodynamic principles, merits, and drawbacks of the technique were provided by Chang et al (1).

Cenotectic measurements

In our isochoric measurements, we encountered two varieties of eutectic pressure-temperature profile, monotonic (Na_2CO_3, KCl, $MgSO_4$, Na_2SO_4, and Urea), and non-monotonic (NaCl, $MgCl_2$, and $NaHCO_3$).

For monotonic profiles, shown in Figures 2.a and 2.b, the cenotectic temperatures and pressures were readily identified by the discontinuity in the eutectic curves, whereupon the liquid / ice Ih / solute-bearing solid phase eutectic configuration transitions to the ice Ih / ice III / solute-bearing solid phase eutectic configuration. In order to more precisely identify the T-P coordinates of the cenotectic invariant point, at which all four phases may coexist, we fit polynomials to each of the eutectic configurations and calculated their intersection (details in Methods). Average cenotectic temperatures and pressures across n = 3 trials per solution are listed in Table 1, alongside the initial concentration of the solution used, the eutectic temperature measured at atmospheric pressure, and the temperature delta between the eutectic and the cenotectic. Standard deviations are included in parentheticals, and this data will be discussed further below.

In Figure 2.a, we also compare our eutectic P-T results for $MgSO_4$ and Na_2SO_4 to those of Hogenboom and colleagues (2, 3), which agree well and represent the only other data we were able to identify on high-pressure low-temperature eutectic equilibria for the systems studied here. Furthermore, although Hogenboom and co. did not measure the cenotectic points of these two solutions, we may estimate them by quadratically fitting the data clusters along the ice Ih eutectic and ice III eutectic lines and calculating the intersections of these fits. Given the notable scatter in the reference data (2, 3), the uncertainty accompanying this calculation is high— but even as such, the cenotectic values calculated from the data of Hogenboom and co. ($MgSO_4$: 211.74 MPa, 248.50 K; Na_2SO_4: 208.34 MPa, 249.95 K) stand in strong agreement with the measurements featured in Table 1.

These literature data also highlight the distinct enhancement in granularity afforded by isochoric freezing, which enables continuous generation and measurement of pressure in response to continuous variation of the temperature, as compared to isobaric techniques performed at discrete isothermal-isobaric pressure-temperature steps. The results herein furthermore confirm the suspicions of Hogenboom et al. that their measurements of water-Na_2SO_4 eutectic coordinates

did not reflect the equilibrium state (i.e. entered a metastable configuration) at pressures above 200 MPa.

Table 1. Measured multiphase T-P equilibria for solutions exhibiting monotonic T-P eutectic curves.

Solute	Initial concentration (wt %)	Eutectic Temperature at 0.1 MPa (K)	Cenotectic Temperature (K)	ΔT from Eutectic at 0.1 MPa (K)	Cenotectic Pressure (MPa)
Na_2CO_3	5.88	270.68 (0.08)	247.49 (0.79)	23.19	217.65 (0.35)
KCl	19.50	262.48 (0.05)	239.12 (0.36)	23.36	210.72 (3.27)
$MgSO_4$	17.30	269.44 (0.02)	247.46 (0.09)	21.98	209.38 (0.17)
Urea	32.80	261.71 (0.03)	240.56 (0.1)	21.15	210.61 (0.52)
Na_2SO_4	4.15	272.09 (0.09)	247.83 (0.24)	24.26	213.71 (3.22)

For NaCl, $MgCl_2$, and $NaHCO_3$, our ability to observe the stable ice III (or ice II below 238 K) transition and determine the cenotectic was confounded by the emergence of previously unknown high-pressure intermediate phases. T-P coordinates measured for each of these systems under different cooling protocols (see Methods) are shown individually in Figure 2.c, and demonstrate the newly realized utility of isochoric freezing as an effective technique for screening for new phases in low-temperature aqueous systems.

In 23.3% NaCl solution, which begins in a eutectic configuration comprised of liquid, ice Ih, and hydrohalite ($NaCl-2H_2O$, or SC2), a phase transition was observed at approximately 237K / 140 MPa, remarkably close to the temperature at which Journaux et al. estimate the recently discovered hyper-hydrate $2NaCl-17H_2O$ (SC8.5) may form(5). This second phase configuration continued without interruption to approximately 215 MPa across trials, but achieved this pressure at between 216 and 224K depending on the run. The P-T coordinates of the initial eutectic configuration agree well with previous data from Kanno & Angell (black triangles in Fig. 2c), who observed high-pressure eutectic phenomena whilst studying pressurized homogeneous ice nucleation via differential thermal analysis in emulsified water-NaCl samples (4). They do not report an additional phase transition however, which is likely a kinetic consequence of both emulsification and miniscule sample sizes (0.04-0.08 mL), which they deploy in order to hinder heterogeneous nucleation of new phases. The large sample sizes (here 5.33 mL) deployable in isochoric freezing may provide a distinct advantage in this regard, helping to ensure timely heterogeneous nucleation of new phases.
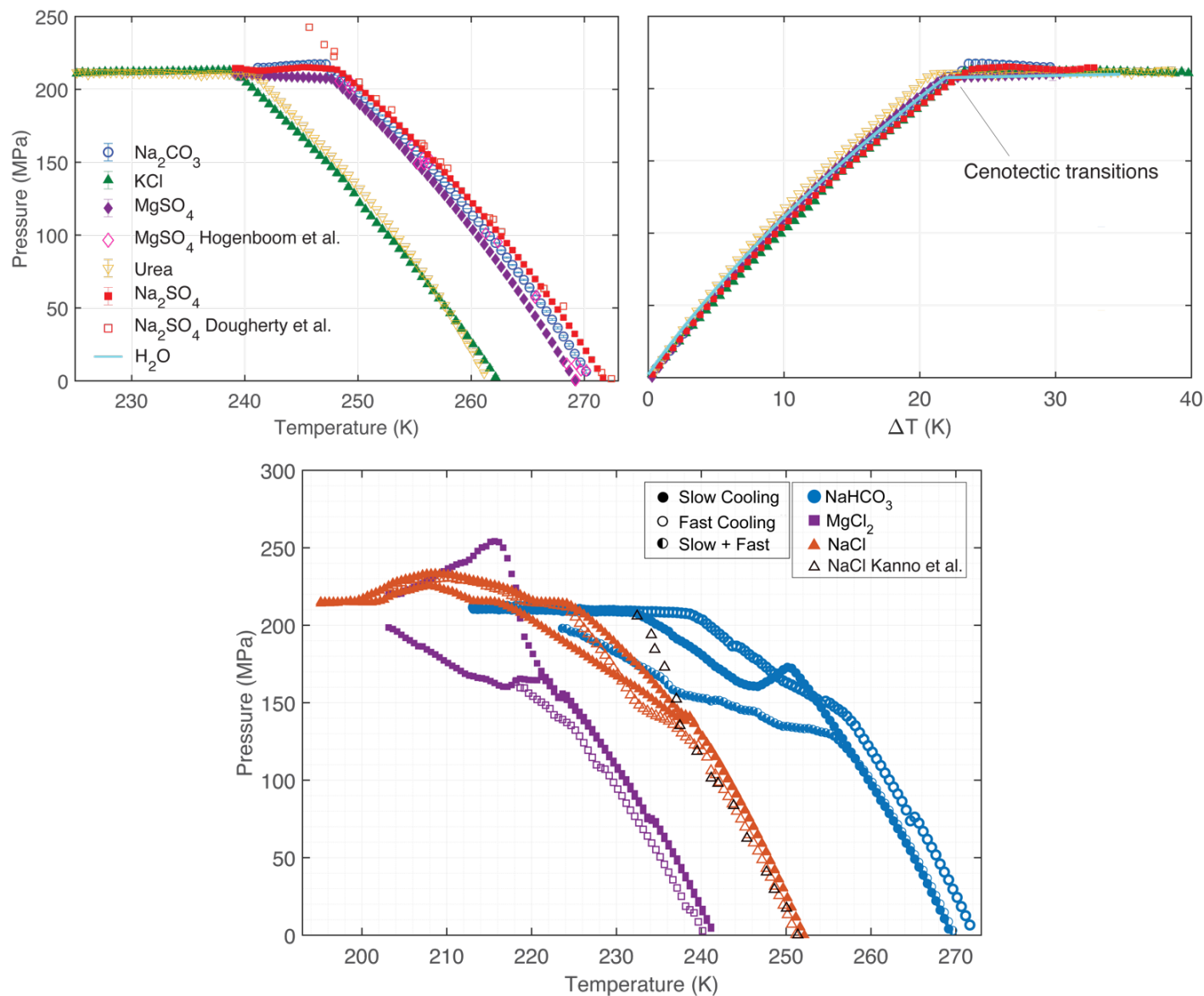
Figure 2. Binary solution eutectic pressure-temperature (P-T) profiles. *a)* P-T profiles for the five binary eutectic solutions tested that do not produce new solute-bearing solid phases at high pressure. The cenotectic point for each solution, or the limit of liquid stability, occurs at the discontinuity in each curve, at which point the remaining liquid solidifies into a solid solution of ice Ih, ice III or ice II, and the solute-bearing solid phase. *b)* the same pressure profiles plotted against the temperature delta from the melting point of ice Ih, which for each of the solutions is the atmospheric pressure eutectic point, and for pure water is 273.15K. In a) and b), markers present the mean of n = 3 replicate trials, and error bars show standard deviation (which is on the order of ~1 MPa across trials). *c)* P-T profiles for three binary eutectic solutions that do produce new solute-bearing solid phases at high pressure. With decreasing temperature, discontinuities in the P-T curve represent phase transitions involving the solute. Each curve represents a single trial, produced via either a slow cooling, fast cooling, or combined slow and fast cooling routine (details in Methods). The variability in P-T trajectory between trials of the same solution using the same cooling protocol, in addition to the sensitivity to cooling protocol and the relaxation of the Clapeyron slope after phase transition, all suggest that the configurations produced in these trials produce new metastable

solute-bearing phases. Further detail on these trials is available in Supplementary Notes 2 and 3, and additional data recorded for the solutions producing intermediate phases is provided in Supplementary Figures S3-S5.

In 6.15% $NaHCO_3$ solution, which begins in a eutectic configuration comprised of liquid, ice Ih, and pure $NaHCO_3$, a phase transition was observed at approximately 255K / 130 MPa, suggesting the existence of the first reported hydrate for $NaHCO_3$, at high-pressure or otherwise. Chamber-to-chamber T-P results grow less consistent after this first phase transition, with two runs eventually unifying in pressure at 210 MPa (albeit at 232K and 238K), and the third taking a much shallower approach in temperature. The transition at 210 MPa suggests that another phase transition may occur in this 232-238K temperature range, be it within the solute-bearing solid phase or the ice phase. Future work should address the structure and stability range of these (potentially multiple) new hydrates, and may provide fundamental new insight into the hydration dynamics of NaHCO3.

Finally, in 21.6% $MgCl_2$ solution, which begins in a eutectic configuration comprised of liquid, ice Ih, and $MgCl_2$-$12H_2O$, discrete phase transitions were observed in multiple runs at approximately 233K / 75 MPa and 223K / 155 MPa, after which the behaviors of the different samples diverged significantly. $MgCl_2$ is known for its diverse array of stable hydrate phases, with hydration numbers up to 12 observed at ambient pressure(6). However, to our knowledge, the only hydrate reported to exist in equilibrium with ice Ih is MgCl2-12H2O, suggesting that the phase transitions observed here may represent previously unrealized phases.

Discussion

Role of water-ice stability in prescribing the cenotectic
Our measurements provide several key insights into the evolution of aqueous systems with pressure. Firstly, it appears that for binary salt systems that do not undergo transitions to a solute-bearing solid phase at high pressures, the T-P coordinates of the cenotectic are dictated nigh-exclusively by the thermodynamics of water/ice. As shown in Fig. 2.b, the P-T evolution of each eutectic configuration from its 0.1 MPa eutectic point precisely mirrors the P-T evolution of ice Ih and liquid water from 273.15K, consistently producing the ice III transition (which here marks the cenotectic) at approximately 22K beneath the melting point of ice Ih, and at approximately 210 MPa. This is a key finding for analysis of binary aqueous salt systems of relevance to planetary science, cryopreservation, etc., providing a thermodynamic limit on the presence of stable equilibrium liquid. We furthermore hypothesize that if no new stable hydrate phases are present at high pressures in *any* given aqueous salt solution, be it a binary or many-component system, this 22K rule should hold true for the temperature difference between the 0.1 MPa univariant eutectic and the cenotectic. Following this logic, as the ice Ih-III-II triple point is located around 238 K and 210 MPa, systems with 1 bar eutectics > 260 K (238+22) are predicted to possess a cenotectic at the Ih-III-solution triple point, and systems with 1 bar eutectics < 260 K are predicted to possess a cenotectic at the Ih-II-solution triple point. We suspect that this fundamental dominance of water-ice thermodynamics over the trajectory of the univariant (here binary eutectic)

configuration is a function of the uniquely high phase volume difference between liquid water and ice Ih, which renders them significantly more sensitive to pressure (in this temperature range) than the solute-bearing solid phases.

Intermediate solute-based phase transitions along the eutectic line
As shown in Fig. 2c., three binary systems that produced intermediate phase transitions within approximately 22K of their 0.1 MPa eutectic points proceeded to diverge from the eutectic trajectories of their monotonic counterparts.

Unlike in the previous solutions, these binaries showed notable sensitivity to the cooling and warming protocol employed and divergence amongst like samples, producing anomalous P-T curves. At equilibrium, a stable phase will have the highest melting temperature at a fixed pressure and composition (or conversely the highest pressure at a fixed temperature and composition). Proceeding along the eutectic curve (toward lower temperatures and higher pressures), if reaching the range of stability of a new hydrate, one should expect a discontinuity in the P-T trajectory, with the value of the Clapeyron slope becoming more negative (steeper). Here we observe the opposite, with the slope becoming more positive (less steep) after discontinuity. This suggests that possible metastable phases of hydrates may have formed during cooling, and that during warming (when step-wise T-P data is recorded), these various phases may reach their metastable melting point(s) below the cenotectic temperature, therefore creating the complex isochoric path we report here.

For example, for the H2O-NaCl system, several new hydrates have recently been reported, including $NaCl \cdot 8.5(H_2O)$ (SC8.5), which possesses a melting point measured at 240K at 380 MPa, and an extrapolated 1 bar metastable melting point at 235K(5). Along the NaCl(aq) isochoric P-T trajectory we see a discontinuity at approximately 140MPa and 238K. This is where one would expect SC8.5 to cross its metastable melting curve at that pressure. This illustrates how a hydrate, stable at higher pressure, can leave a clear trace as a metastable phase in an isochoric experiment. Accordingly, this suggests that the other systems with anomalous isochoric paths possess other undiscovered hydrates, potentially stable at higher pressures. This supports the hypothesis of pressure-induced hydrate structural diversity (hyper-hydration) from Journaux et al.(5), and we expect one or multiple new hydrates to be stable at higher pressures in $MgCl_2$ and $NaHCO_3$. This underlines the power of the isochoric method to rapidly explore the fundamental thermodynamics and physical chemistry of these systems, and future experiments should investigate high pressure stability and structure of hydrates in those systems.

Finally, it should be noted that formation of metastable intermediates confounds our ability to directly measure the stable cenotectic temperature in these chemical systems. This presents an interesting physical paradox: new hydrates encountered along the eutectic curve that originates at 0.1MPa must definitionally be *stable* at *higher* pressures than the eutectic P-T curve would provide; but as observed, they may produce *metastable* configurations at *lower* pressures. This implies that the formation of new *stable* hydrates, at thermodynamic equilibrium, will *increase* the cenotectic temperature, ushering the system to pressures at which ice II or III may form at higher temperatures (less than the 21K rule of thumb) and limiting the stability range of the liquid.

Simultaneously, the formation of *metastable* new hydrates will *decrease* the cenotectic temperature, extending the temperature range over which liquid may exist by tens of degrees or more (Fig. 2c).

Implications for materials thermodynamics and generalized definition of the cenotectic

For any thermodynamic system, under the influence of any arbitrary selection of physical or chemical thermodynamic forces (pressure, chemical potential, etc.) acting at arbitrary intensities, there exists a temperature limit to the stability of the liquid phase, which we here dub the cenotectic. For systems free of the influence of non-simple modes of thermodynamic work (e.g. magnetic work, electronic work, stress-strain work, surface work, etc.), this limit will be a function of pressure and $c - 1$ compositional variables, wherein c is the number of chemical components. For systems under the influence of the more exotic forms of thermodynamic work mentioned above, the cenotectic will depend further on one additional variable for each contributing work mode. As such, this cenotectic limit is a fundamental material property of the system, yet, outside of chemically pure systems, it has seldom (if ever) been precisely characterized.

In this work, we have measured the cenotectic for a variety of binary salty aqueous systems. However, these systems represent just one of several phenomenological profiles that the cenotectic may possess. Because mechanical (PV) work affects all thermodynamic systems, the cenotectic will always occur at the intersection of two univariant phase lines with opposite-signed Clapeyron (dP/dT) slopes, regardless of chemical complexity or the role of other thermodynamic fields. For the systems tested here, because water produces a solid phase (ice Ih) less dense than the liquid (thereby providing a negative Clapeyron slope along its liquidus curve), and because the eutectic featuring ice Ih is the lowest-temperature eutectic in the atmospheric pressure phase diagram, the cenotectic logically falls at the intersection of two univariant liquid-solid-solid equilibrium lines, one involving ice Ih (plus the solute-bearing solid phase) and the other involving an ice phase (II or III) more dense than the liquid (plus the solute-bearing solid phase). This reasoning can be applied equally to other systems with negative Clapeyron slope melting curves, for which the cenotectic can fall along the solid-solid transition to the denser phase (which is usually quasi-isobaric). We therefore predict that the cenotectic pressure can be expected to be approximately 11-12 GPa for many silicon solutions, 1.5 GPa for many gallium solutions, and 5-10 GPa for many carbon solutions.

However, for most binary material systems, which do not possess a solid phase less dense than the liquid along the eutectic line, the negative-Clapeyron phase line leading into the phase intersection marked by the cenotectic will generally include liquid-vapor-solid equilibrium, instead of liquid-solid-solid equilibrium. Likewise, in aqueous solutions for which the lowest-temperature eutectic at atmospheric pressure does *not* involve ice Ih, such as methanol (7), DMSO (8), and etc., the cenotectic may also occur at the intersection of a liquid-vapor-solid (negative Clapeyron slope) line and a liquid-solid-solid (positive Clapeyron slope).

Generally, the cenotectic point of a system will behave one of two ways, depending upon the densities of the phases involved. If the lowest-temperature eutectic at atmospheric pressure

involves a phase less dense than the liquid, the cenotectic will likely occur at increased pressures, and generally at the intersection of negative-Clapeyron and positive-Clapeyron liquid-solid-solid equilibrium lines. This is the case applicable to all of the systems studied here, and the case we suggest should be broadly applicable to aqueous salt systems writ large. Alternatively, if the lowest-temperature eutectic at atmospheric pressure involves only phases that are denser than the liquid, the cenotectic will likely occur at *decreased* pressures, and generally at the intersection of a positive-Clapeyron liquid-solid-solid and a negative-Clapeyron liquid-vapor-solid line. This appears to be the case for example in the water-methanol system (7), for which the lowest temperature eutectic at 1 bar does not include ice Ih, but instead solid methanol and its monohydrate. Note however that for systems with multiple eutectics at similar temperatures (such as water-DMSO), the specific pressure-dependences of the solid phases involved may affect which 1 bar eutectic the cenotectic will originate from, and an *a priori* determination of the phases involved may not be feasible.

It must also be noted that the number of phases present in the univariant phase lines that intersect to form the cenotectic will increase with the number of chemical components in the system, per the classical Gibbs Phase Rule, and with the number of additional thermodynamic fields (strain, magnetic, electric, etc.) acting upon the system, per the Generalized Gibbs Phase rule(9), leaving many exciting multiphase configurations to characterize across varying thermodynamic systems.

We suggest that establishment and exploration (both experimental and theoretical) of the cenotectic concept is vital to rigorous understanding of the thermodynamics of modern materials systems, which exist under increasingly complex chemical-thermodynamic conditions and produce increasingly rich multi-phase equilibria(10–13). For the benefit of the modern student of thermodynamics, we thus conclude our thermodynamic discussion with a formal definition of the cenotectic:

The cenotectic is the invariant point occurring at the lowest temperature at which the liquid phase, for any value of concentration, pressure, or other thermodynamic forces acting on the system, remains in stable equilibrium.

Implications for planetary science

In icy ocean worlds such as Europa, Enceladus, Titan, Ganymede, Ceres, Pluto and potentially moons of Uranus Ariel, Umbriel, Titania and Oberon (14–16) the coordinates of the eutectic controls the stability and circulation of briny fluids in the icy crust, and the formation behaviors of the top boundary of their ocean. With increasing pressure, the temperature of the eutectic will decrease in the ice Ih crust (Fig. 3). Several studies in recent years have underlined the importance of brine percolation and brine connectivity in vertical transport through the ice crust under chaos regions(17), double ridge formations(18), or impacts and cryo-volcanism(19–21). The extent to which brines formed near the surface can percolate through the ice shell by various mechanisms and act as nutrient sources for the underlying oceanic habitat is *in-fine* controlled by the eutectic coordinates (Figure 3). The present work allows us to demonstrate that for a pressure of the bottom of the icy shell of 50 MPa(15, 22) eutectic temperature of aqueous systems can be

depressed by up to 4-5 K compared to its 1 bar value. This difference is significant, and could enhance fluid circulation in thick ice crusts(17, 23), further facilitating vertical transport of oxidant/nutrients from the surface to the ocean. The high-pressure behavior of the eutectic is also relevant to the base of the ice shell, especially in controlling the formation, thickness, and chemical gradients of ocean interface mush(24, 25) (Fig. 3), and possible briny habitats(26).
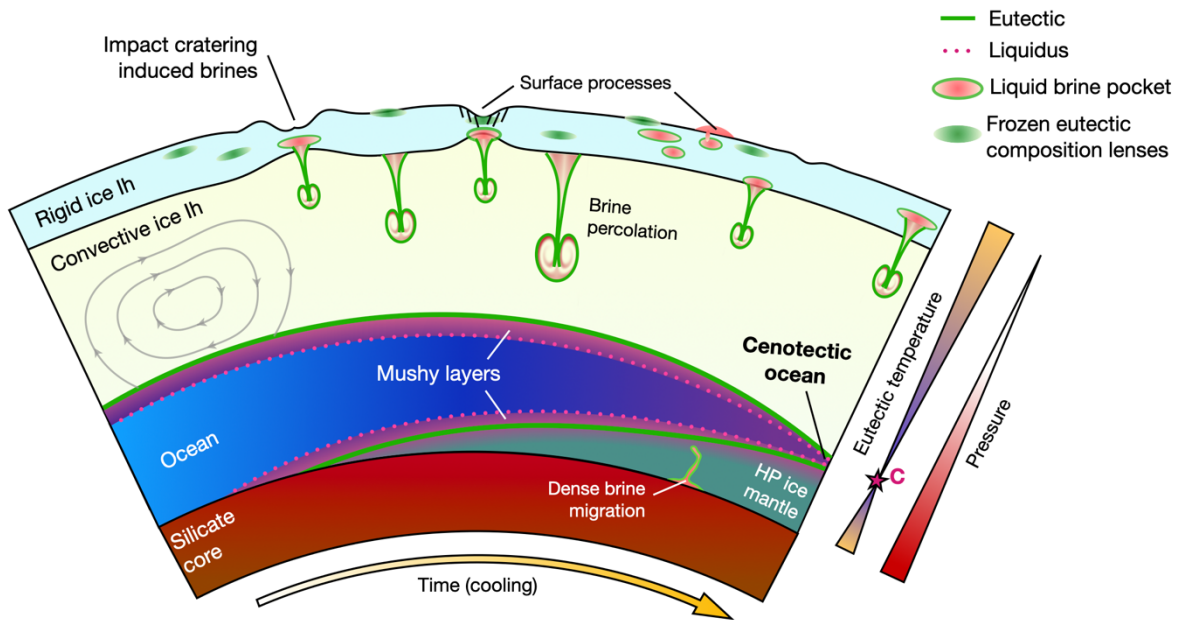

Figure 3. Schematic interior structure of an icy moon and the various geological processes involving the eutectic and the cenotectic (C). Ice Ih layer relative thickness is exaggerated for clarity.

The behavior of the eutectic line at pressures higher than the cenotectic, in equilibrium with high pressure ice polymorphs, remains to be studied with other techniques. Nonetheless, a reasonable assumption is to expect a similar behavior to that at low pressure, i.e. following the overall shape of the high pressure ices melting curves with a given ΔT, if no high pressure hydrates are present (Fig. 2b). For aqueous salt systems with cenotectic temperatures colder than 238 K, ice II should form and the eutectic will follow the ice II-aqueous fluid melting line, which remains to be measured experimentally for most relevant solutions. To our knowledge, ice II melting curves are only available for a few select solutes, including aqueous ammonia and aqueous methanol (7, 27).

For large icy ocean worlds with high-pressure ices (e.g. Ganymede, Titan, Callisto) and ocean exoplanets, the coordinates of the eutectic line will also control the circulation of metamorphic fluids or fluids from hydrothermalism through the high pressure ice mantle, and dictate the possibility of vertical exchange of nutrients from the rocky core towards the ocean (Figure 3). These processes and possibilities are discussed in references (28–33).

Finally, the cenotectic plays a major role in planetary oceans "endgame" for these same large water-rich planetary bodies, such as icy moons, cold ocean exoplanets, and water-rich rogue planets. As these bodies cool over geologic timescales, or with loss of internal heating such as

tidal dissipation or radiogenic heating, their oceans will gradually freeze from top and bottom (Fig.3), until complete solidification is achieved. This happens in the case that the density of the aqueous solution stays lower than high pressure ices, which depends on the solute molar mass and the composition of the eutectic. Otherwise the brine could be transported downward and may form dense basal oceans(33–35). In the following discussion we assume that the brine at the cenotectic remains buoyant compared to high pressure ices. This important density inversion effect, which could control the distribution of aqueous reservoirs in water-rich planetary bodies, requires further investigation into the composition and density of aqueous systems along the eutectic and at the cenotectic. We also assume that all of the chemical constituents dominating the composition of these icy oceans possess high-pressure cenotectics, like the salt systems studied here, and that the aqueous solutions always remain buoyant compared to high pressure ices.

For cold water-rich planetary bodies, the last remnant liquid layer will occur at the depth corresponding to the pressure of the cenotectic (P_c), as shown in the present study to be around 210 MPa. In Figure 4, this cenotectic depth z_c of the last ocean is presented as a function of gravity, and discrete values are reported in Table 2. Cenotectic depth is estimated using the formula $z_c = P_c/(\rho \cdot g)$, with the density ρ of the overlying ice taken at 930 kg/m3 (the average value for an adiabatic thermal profile in an ice Ih crust around 250K [Journaux et al. 2020]), and g taken as the surface gravitational acceleration of the planetary body. Bodies with smaller gravity will have their last remaining liquid at greater depth, over 150 km for all large icy moons in our solar system. Small objects like Ceres, Pluto, and others are omitted here, as the calculated depth of the cenotectic is shallower than the estimated thickness of their hydrospheres. For Europa, the depth of the cenotectic roughly corresponds to the estimated thickness of its hydrosphere. For larger icy moons, the final ocean will be sandwiched between layers of ice Ih and ice III or ice II, depending on the precise composition of the remaining briny liquid. Interestingly, the depth of the cenotectic also provides the absolute maximum upper limit for the ice crust thickness if an ocean is present, which is 172 km for Titan, and 158 km for Ganymede. For larger bodies such as water rich exoplanets, the depth of the final ocean will be shallower, with depth ranging from 28 km for TRAPPIST-1 e to 9.7km for LHS 1140 b, implying much thinner maximum ice Ih crust (<30km) for cold ocean super earths.

Table 2: *Cenotectic depth for various relevant icy moons of our solar system and ocean exoplanet candidates with effective surface temperatures below 273K.*

| Object	Surface Gravity (m/s^2)	Depth of the cenotectic (km) (i.e. last ocean)
Callisto	1.24	182
Titan	1.32	172
Europa	1.35	167
Ganymede	1.43	158
TRAPPIST-1 e	7.98	28
TRAPPIST-1 f	9.41	24
1g_E exoplanet	9.81	23
Teegarden's Star c	10.04	22.5
TRAPPIST-1 g	10.12	22.3
Proxima Cen b	10.6	21.3
GJ 667 C f	11.82	19.1
GJ 667 C e	11.82	19.1
GJ 1061 d	12.14	18.6
Keppler-186 f	12.23	18.5
Keppler 2-18b	12.43	18.2
Keppler-442 b	12.68	17.8
Keppler-1229 b	12.68	17.8
LHS 1140 b	23.22	9.7
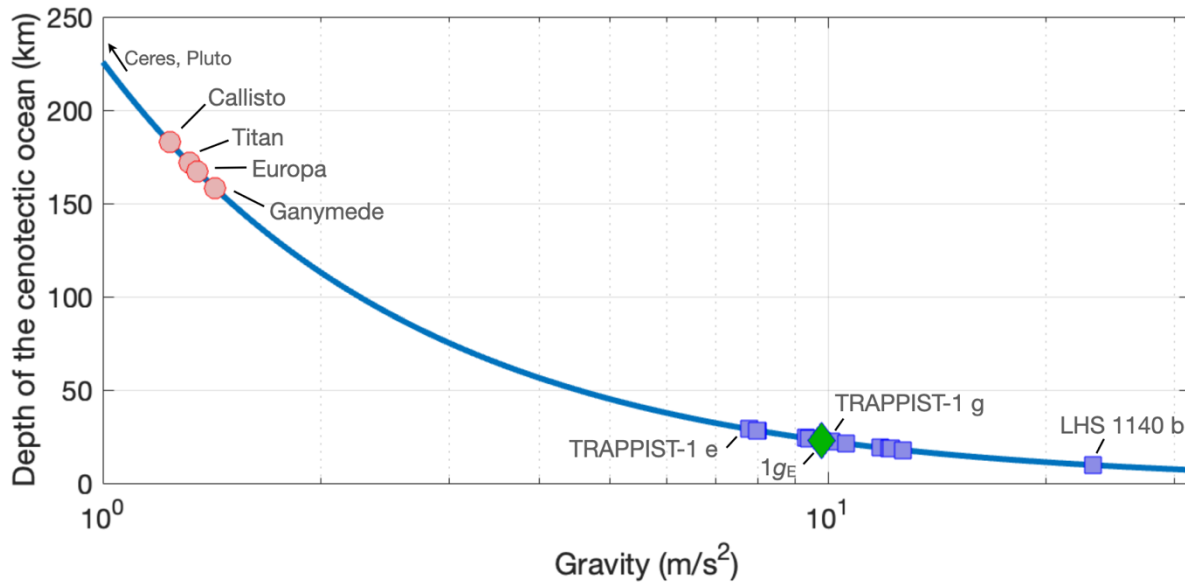
Figure 4: Evolution of the depth of the final ocean (cenotectic depth) for different planetary bodies from our solar system and ocean exoplanet candidates.

Implications for cryopreservation

Cryopreservation research has surged into a period of renaissance in the past decade, and many exciting new medicine- and conservation-oriented cryopreservation efforts are driven by advances in aqueous thermodynamics(36) and thermal physics(37). Similar to current planetary science efforts, the ability to explore new thermodynamic techniques and parameter spaces is limited by state-of-the-art knowledge of low-temperature phase equilibria, including in the multi-phase and high pressure regimes.

For example, naturally-occurring deep-eutectic systems (NADES), which rely upon eutectic crystallization to minimize extracellular mechanical and osmotic damage(38), have emerged as a standout for cell therapy preservation(39, 40); isochoric freezing(41) and vitrification(36), which leverage both nano- and macro-scale pressure-effects in confined aqueous systems, have enabled cryopreservation of mature coral fragments and prolonged cold storage of fresh foods(42); hyperbaric vitrification provided key early demonstrations of whole organ vitrification(43); and so on. The cenotectic data presented here establish initial thermodynamic limits in temperature and pressure that can aid in exploring and refining these emergent techniques, and furthermore underscore the need for similar measurements as conducted here in solutions of common cryoprotectants such as glycerol, ethylene glycol, DMSO, sucrose, glucose, and etc.

Concluding Remarks

The cenotectic, or the invariant point defining the lowest temperature at which a liquid remains stable under any possible values of concentration, pressure, and other thermodynamic parameters affecting the system, is an important concept in material characterization of complex multiphase systems. As the thermodynamic and compositional parameter spaces of interest to

the research community grow ever larger, identifying globally limiting behaviors becomes increasingly essential, and we suggest that the cenotectic concept may help to establish definite and fundamental limits on liquid phase equilibria. With that in mind, future research should aim not only to measure the cenotectic limits of many other chemical systems, but to further refine and explore the concept itself, with the goal of ever deeper understanding of the physical limits of material systems.

Methods:

Isochoric Freezing Process

In order to identify the temperature limit of liquid stability in the aqueous solutions explored herein, we employed the isochoric freezing technique reported previously by Chang et al. In brief, 5.33 mL aqueous samples mixed at the atmospheric-pressure eutectic concentration were confined absent air within a custom Al7075 isochoric chamber fitted with a high-pressure transducer (ESI Technology Inc). By constraining the total volume of the binary system and allowing the pressure to vary freely, we create a thermodynamic environment in which the 3-phase equilibrium present in the eutectic configuration is prescribed by a single intensive thermodynamic degree of freedom. As such, temperature and pressure are coupled within the chamber, and simple control of the temperature enables simultaneous measurement of the equilibrium temperature and pressure. Further experimental details and chamber schematics are provided in Supplementary Note 1.

Cooling process

Two high-accuracy recirculating cooling baths were employed for isochoric testing, a PolyScience AP15R-40 with a minimum working temperature of 243.15K and a Fluke Calibration 7380 with a minimum working temperature of 193.15K. The latter was utilized for solutions with phase transitions lower than 243.15K (including all those exhibiting intermediate high-pressure hydrate phases), and the former for all others. For each solution, three replicate samples in identical chambers were studied, and the chambers are submerged completely within the cooling bath fluid to ensure uniformity of temperature. More details on the cooling methodology are available in Supplementary Note 1, and a sample cooling profile is shown in Supplementary Note 2.

For solutions without intermediate high-pressure hydrates phases, the employed cooling procedure mirrored that detailed previously by Chang et al. In this approach, the chambers are plunged into a bath pre-cooled to at least 30K beneath the 0.1 MPa eutectic temperature of the solution, allowed to stabilize for 45 minutes (a time period chosen to ensure initiation of the ice III transition, indicated upon cooling by a precipitous collapse in pressure to approximately 210 MPa), then warmed in increments of 0.5K per 45 minute. This increment was deemed to produce steady steady-state P-T data by the end of each step (at which point the data is sampled), as indicated by a <0.1 MPa/min evolution of the pressure.

For solutions found to host intermediate high-pressure hydrate phases (NaCl, NaHCO$_3$, and MgCl$_2$), contrary to their less phase-diverse counterparts, preliminary testing showed broad varieties in behavior sample-to-sample, leading us to believe that metastable configurations were being produced and that a more gradual cooling approach was necessary. As such, for the protocol identified as "Slow Cooling" in Figure 2c., the chambers were pre-cooled only to 273.15K, and the bath temperature was then decreased by 1K every 10 minutes. The protocol identified as "Fast Cooling" follows the previously described approach of Chang et al., wherein the chamber is submerged directly into liquid pre-cooled to the minimum temperature of the run. In order to demonstrate the hallmark dependence of metastable configurations on thermal history, a combined slow-fast cooling approach was also tested, which incorporated a pseudo-annealing logic. In this process, the temperature was incrementally lowered at a rate of 1K per 10 minutes

until the intermediate hydrate was detected, then raised 5K above the observed transition temperature and cooled once more at a rate of 0.6K/min to the cenotectic point.

Warming process

For all solutions, after completion of the cooling process, the system is heated in discrete increments of 0.5K, each held for 20 minutes to allow phase equilibration. The steady pressure and temperature are recorded at the end of each step, and this pressure-temperature data provides the P-T curves shown in Figure 2.

Eutectic and Cenotectic Point Identification

In order to extract more precise cenotectic points from the P-T data shown in Figure 2.a, second-order polynomials were fit to the data above and below the apparent cenotectic temperature (as indicated by the discontinuity in the P-T curve) using the polyfit() function in MATLAB, and their intersection provided the cenotectic temperatures/pressures reported in Table 1.

Similarly, following the approach of Chang et al.(1), the intersection of the higher-temperature fitted polynomial curve with the 0.1 MPa isobar identifies the atmospheric pressure eutectic temperature of system.

Competing Interests Statement: The authors acknowledge no competing or conflicting interests.

Data Availability Statement: All data reported herein are available in tabular form in the Supplementary Data Appendix. Any additional information sought may be requested from the corresponding authors.

Code Availability Statement: All code employed for the analysis of data herein is available upon reasonable request to the corresponding authors. We will note however that only standard MATLAB curve fitting functions were employed, and no custom scripts were developed for analysis.

References:

1.   B. Chang, *et al.*, On the pressure dependence of salty aqueous eutectics. *Cell Reports Phys. Sci.* **3**, 100856 (2022).

2.   D. L. Hogenboom, J. S. Kargel, J. P. Ganasan, L. Lee, Magnesium sulfate-water to 400 mpa using a novel piezometer: Densities, phase equilibria, and planetological implications. *Icarus* **115** (1995).

3.   J. S. Dougherty, A. J. ; Avidon, J. A. ; Hogenboom, D. L. ; Kargel, Eutectic Temperatures for Low and High Pressure Phases of Sodium Sulfate Hydrates with Applications to Europa in *43rd Lunar and Planetary Science Conference, LPI Contribution No. 1659, Id.2321*, (2012).

4.   H. Kanno, C. A. Angell, Homogeneous nucleation and glass formation in aqueous alkali halide solutions at high pressures. *J. Phys. Chem.* **81**, 2639–2643 (1977).

5.   B. Journaux, *et al.*, On the identification of hyperhydrated sodium chloride hydrates, stable at icy moon conditions. *Proc. Natl. Acad. Sci.* **120** (2023).

6.   K. Yamashita, K. Komatsu, T. Hattori, S. Machida, H. Kagi, Crystal structure of a high-pressure phase of magnesium chloride hexahydrate determined by *in-situ* X-ray and neutron diffraction methods. *Acta Crystallogr. Sect. C Struct. Chem.* **75**, 1605–1612 (2019).

7.   A. J. Dougherty, *et al.*, The Liquidus Temperature for Methanol-Water Mixtures at High Pressure and Low Temperature, With Application to Titan. *J. Geophys. Res. Planets* **123**, 3080–3087 (2018).

8.   D. H. RASMUSSEN, A. P. MACKENZIE, Phase Diagram for the System Water–Dimethylsulphoxide. *Nature* **220**, 1315–1317 (1968).

9.   W. Sun, M. J. Powell-Palm, Generalized Gibbs' Phase Rule. *arXiv Preprint Server* (2021). https://arxiv.org/abs/2105.01337

10.   J. Potticary, *et al.*, An unforeseen polymorph of coronene by the application of magnetic fields during crystal growth. *Nat. Commun.* (2016) https:/doi.org/10.1038/ncomms11555.

11.   D. A. Kitchaev, S. T. Dacek, W. Sun, G. Ceder, Thermodynamics of Phase Selection in MnO2 Framework Structures through Alkali Intercalation and Hydration. *J. Am. Chem. Soc.* (2017) https:/doi.org/10.1021/jacs.6b11301.

12.   J. E. Aber, S. Arnold, B. A. Garetz, A. S. Myerson, Strong dc electric field applied to supersaturated aqueous glycine solution induces nucleation of the γ polymorph. *Phys. Rev. Lett.* (2005) https:/doi.org/10.1103/PhysRevLett.94.145503.

13.   M. Bianchini, *et al.*, The interplay between thermodynamics and kinetics in the solid-state synthesis of layered oxides. *Nat. Mater.* **19** (2020).

14.   F. Nimmo, R. T. Pappalardo, Ocean worlds in the outer solar system. *J. Geophys. Res. Planets* **121** (2016).

15.   S. D. Vance, *et al.*, Geophysical Investigations of Habitability in Ice-Covered Ocean Worlds. *J. Geophys. Res. Planets* **123** (2018).

16.   J. Castillo-Rogez, *et al.*, Compositions and Interior Structures of the Large Moons of Uranus and Implications for Future Spacecraft Observations. *J. Geophys. Res. Planets* **128** (2023).

17.   M. A. Hesse, J. S. Jordan, S. D. Vance, A. V. Oza, Downward Oxidant Transport Through Europa's Ice Shell by Density-Driven Brine Percolation. *Geophys. Res. Lett.* **49** (2022).

18.   R. Culberg, D. M. Schroeder, G. Steinbrügge, Double ridge formation over shallow water sills on Jupiter's moon Europa. *Nat. Commun.* **13** (2022).

19.   G. Steinbrügge, *et al.*, Brine Migration and Impact-Induced Cryovolcanism on Europa. *Geophys. Res. Lett.* **47** (2020).

20.   E. Lesage, H. Massol, S. M. Howell, F. Schmidt, Simulation of Freezing Cryomagma Reservoirs in Viscoelastic Ice Shells. *Planet. Sci. J.* **3** (2022).

21.   E. Lesage, H. Massol, F. Schmidt, Cryomagma ascent on Europa. *Icarus* **335** (2020).

22.   B. Journaux, *et al.*, Large Ocean Worlds with High-Pressure Ices. *Space Sci. Rev.* **216**, 7 (2020).

23.   K. Kalousová, O. Souček, G. Tobie, G. Choblet, O. Čadek, Ice melting and downward transport of meltwater by two-phase flow in Europa's ice shell. *J. Geophys. Res. Planets* **119** (2014).

24.   J. J. Buffo, B. E. Schmidt, C. Huber, C. R. Meyer, Characterizing the ice-ocean interface of icy worlds: A theoretical approach. *Icarus* **360** (2021).

25.   J. J. Buffo, B. E. Schmidt, C. Huber, C. C. Walker, Entrainment and Dynamics of Ocean-Derived Impurities Within Europa's Ice Shell. *J. Geophys. Res. Planets* **125** (2020).

26.   N. S. Wolfenbarger, M. G. Fox-Powell, J. J. Buffo, K. M. Soderlund, D. D. Blankenship, Brine Volume Fraction as a Habitability Metric for Europa's Ice Shell. *Geophys. Res. Lett.* **49** (2022).

27.   M. Choukroun, O. Grasset, Thermodynamic data and modeling of the water and ammonia-water phase diagrams up to 2.2 GPa for planetary geophysics. *J. Chem. Phys.* **133** (2010).

28.   B. Journaux, *et al.*, Salt partitioning between water and high-pressure ices. Implication for the dynamics and habitability of icy moons and water-rich planetary bodies. *Earth Planet. Sci. Lett.* **463** (2017).

29.   G. Choblet, G. Tobie, C. Sotin, K. Kalousová, O. Grasset, Heat transport in the high-pressure ice mantle of large icy moons. *Icarus* **285** (2017).

30.   K. Kalousová, C. Sotin, G. Choblet, G. Tobie, O. Grasset, Two-phase convection in Ganymede's high-pressure ice layer — Implications for its geological evolution. *Icarus*

299 (2018).

31.   L. Lebec, S. Labrosse, A. Morison, P. J. Tackley, Scaling of convection in high-pressure ice layers of large icy moons and implications for habitability. *Icarus* **396** (2023).

32.   J. A. Hernandez, R. Caracas, S. Labrosse, Stability of high-temperature salty ice suggests electrolyte permeability in water-rich exoplanet icy mantles. *Nat. Commun.* **13** (2022).

33.   B. Journaux, Salty ice and the dilemma of ocean exoplanet habitability. *Nat. Commun.* **13** (2022).

34.   B. Journaux, I. Daniel, R. Caracas, G. Montagnac, H. Cardon, Influence of NaCl on ice VI and ice VII melting curves up to 6GPa, implications for large icy moons. *Icarus* **226** (2013).

35.   S. Vance, J. M. Brown, Thermodynamic properties of aqueous MgSO4 to 800MPa at temperatures from −20 to 100°C and concentrations to 2.5molkg−1 from sound speeds, with applications to icy world oceans. *Geochim. Cosmochim. Acta* **110**, 176–189 (2013).

36.   M. J. Powell-Palm, *et al.*, Cryopreservation and revival of Hawaiian stony corals using isochoric vitrification. *Nat. Commun.* **14**, 4859 (2023).

37.   A. Sharma, *et al.*, Cryopreservation of Whole Rat Livers by Vitrification and Nanowarming. *Ann. Biomed. Eng.* (2022) https:/doi.org/10.1007/s10439-022-03064-2.

38.   A. Joules, T. Burrows, P. I. Dosa, A. Hubel, Characterization of eutectic mixtures of sugars and sugar-alcohols for cryopreservation. *J. Mol. Liq.* **371**, 120937 (2023).

39.   R. Li, K. Hornberger, J. R. Dutton, A. Hubel, Cryopreservation of Human iPS Cell Aggregates in a DMSO-Free Solution—An Optimization and Comparative Study. *Front. Bioeng. Biotechnol.* **8** (2020).

40.   K. Hornberger, G. Yu, D. McKenna, A. Hubel, Cryopreservation of Hematopoietic Stem Cells: Emerging Assays, Cryoprotectant Agents, and Technology to Improve Outcomes. *Transfus. Med. Hemotherapy* **46** (2019).

41.   M. J. Powell-Palm, B. Rubinsky, W. Sun, Freezing water at constant volume and under confinement. *Commun. Phys.* **3** (2020).

42.   C. Bilbao-Sainza, *et al.*, Preservation of Grape Tomato by Isochoric Freezing. *Food Sci. Int.* (2020).

43.   G. M. Fahy, D. R. MacFarlane, C. A. Angell, H. T. Meryman, Vitrification as an approach to cryopreservation. *Cryobiology* **21**, 407–26 (1984).

Supporting Information for

On the equilibrium limit of liquid stability in pressurized aqueous systems

Arian Zarriz[1], Baptiste Journaux[3^], Matthew J. Powell-Palm[1,2^]

[1]J. Mike Walker '66 Department of Mechanical Engineering, Texas A&M University, College Station, TX, USA

[2]Department of Materials Science & Engineering, Texas A&M University, College Station, TX, USA

[3]Department of Department of Earth and Space Sciences, University of Washington, Seattle, WA, USA

Correspondence:

BJ (bjournau@uw.edu)

MPP (powellpalm@tamu.edu)

This PDF file includes:

      Supplementary Notes S1-S3

      Supplementary Figures S1 to S5

      Supplementary Table S1

      SI References

Supplementary Note 1. Isochoric Freezing Methodology

The isochoric freezing approach employed here is detailed completely in Chang et al. (main text reference 1), but for the aid of the reader seeking to employ isochoric freezing, we will provide a brief overview of the methodology herein.

Isochoric freezing is a thermo-volumetric method used to investigate the phase transitions and equilibria of aqueous solutions. By constraining the volume and concentration of a eutectic binary solution, per Gibbs Phase Rule, the system is forced into a 1-DoF thermodynamic configuration, wherein its equilibrium is fully prescribed by one intensive variable. In practice, the experimentalist controls the temperature, allowing the pressure to respond per Le Chatelier's principle and recording it.

For the binary solutions studied here, the isochoric freezing process proceeds as follows. First, a solution at the 0.1 MPa eutectic concentration is prepared. We used the literature values of atmospheric eutectic concentration listed in Table S1. This liquid is then loaded (absent any air bubbles) into a rigid pressure-bearing Al7075 isochoric chamber (internal volume 5.33 mL) equipped with an ESI GD4200-USB-4000-DE digital pressure transducer (Figs. S1a and S1b). These transducers enable high-fidelity pressure measurements up to 400 MPa, at a sampling frequency of 1 Hz. They are operated via a proprietary "ESI-USB" data acquisition software available from the company.

Upon filling the chamber, the pressure transducer is threaded into the chamber and torqued down to 45 N.m. This torque value ensures effective chamber closure via metal-on-metal surface sealing (as labeled in Figure S1.b), while preventing undue stress on the sensor housing.

Table S1. Atmospheric eutectic concentration for different binary solutions

Solute	Eutectic concentration at 0.1 MPa (wt%)	Reference
Na_2CO_3	5.88	*Pascual, M., et al.*[1]
KCl	19.50	*Li, Gang, et al.*[2]
$MgSO_4$	17.30	*Pillay, Venasan, et al.*[3]
Urea	32.80	*Yuan, Lina, et al.*[4]
Na_2SO_4	4.15	*González Díaz, C., et al.*[5]
NaCl	23.30	*Journaux et al., Drebushchak et al.*[6]
$NaHCO_3$	6.15	*Pascual, M., et al.*[1]
$MgCl_2$	21.60	*Ketcham, S. A. et al.*[7]*, González Díaz, C., et al.*[5]

To maintain controlled temperature conditions for the electronics housed within the pressure transducers during the experiment (independent of the temperature of the chamber/sample), a 13W polyimide film heater with a 70 mm diameter is affixed to each pressure sensor. These heaters are regulated by a simple thermal relay responding to the observed temperature of the transducer's electronics housing, and they are set to maintain a constant temperature of 306.15 ± 0.5K. The relays are powered by a generic 12V DC power supply.

A 3D-printed lid was subsequently constructed to enable mounting of three chambers simultaneously in the bath, facilitating both total immersion of the isochoric chambers within the cooling fluid and insulation of the pressure transducer electronics housing above (Figure S1d/d).

Two cooling baths were employed, as described in the main text. The PolyScience AP15R-40 bath was employed for binary solutions with ice-III transition temperatures higher than 243.15K, while the 7380 Fluke ultra-low temperature bath was utilized to achieve lower temperatures, reaching as low as 193.15K. This setup enabled high-throughput data collection for various binary solutions.

The cooling and warming processes within the Fluke bath were programmed using MATLAB, allowing for easy adjustments as needed. The temperature within the bath was also recorded using a calibration-grade Fluke stick thermometer, which was submerged in the bath near the chambers, to ensure precise temperature measurement.

Each experimental run involved two to three chambers, with distinct freezing protocols implemented to explore the impact of cooling rates on resultant equilibria.
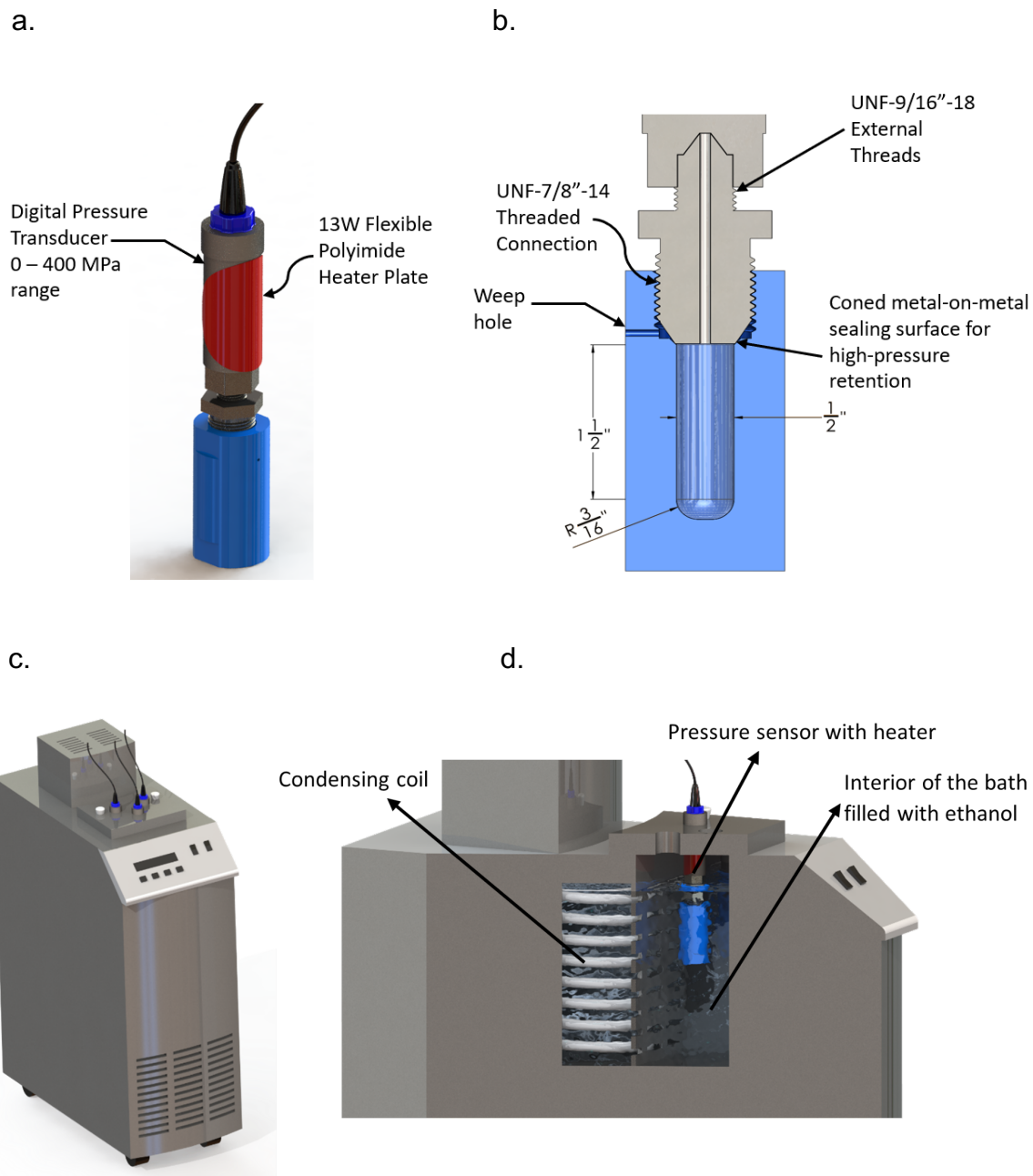
Figure S1: Isochoric freezing assembly. a) 3D render of Al7075 isochoric chamber (blue) and pressure transducer assembly, b) 2D cros-section of isochoric chamber and pressure transducer assembly, c,d) 3D renders of the fully assembled cooling bath, chamber, and pressure transducer assembly.

Supplementary Note 2. Example cooling profile

In order to obtain equilibrium data with the highest degree of confidence possible, the P-T coordinates reported in the main text were acquired upon slow warming of the solutions. However, the general phenomenology of the cooling process may be of interest to the reader seeking to perform isochoric experiments, and we thus provide a typical cooling profile below.
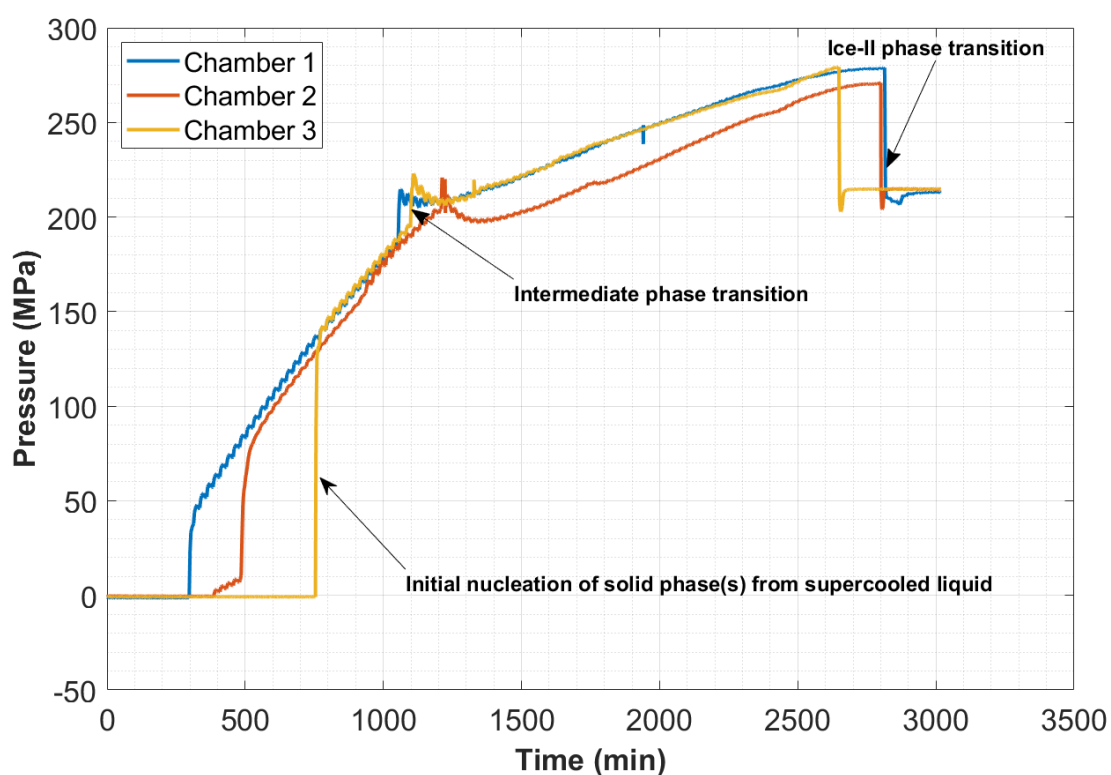

Figure S2. Sample slow cooling protocol for NaCl.

During the slow cooling process depicted in Figure S2, which proceeded from 273.15K to 213.15K over the time course shown, three distinct phase transition events are observed.

In the first several hours of cooling, the chambers supercool to varying degrees, yielding no substantive change in pressure until the nucleation of the solid phases. Note the expected correlation between prolonged period of supercooling and post-nucleation pressure.

Next, an intermediate phase transition is observed, consistent across chambers. This phase configuration, which is suspected to be highly metastable (see discussion in main text), then proceeds to increase in pressure as the temperature decreases, reaching a peak of approximately 280MPa before the collapse to ice II is observed. Note that when this final transition occurs, at approximately 280 MPa and 213.15K, the phase configuration may be metastable with respect to several different phases, i.e., there may be both metastable hydrates and metastable liquid present. Future research should seek to disentangle these sequential metastabilities.

Supplementary Note 3: Additional data for NaHCO3, NaCl, and MgCl2 data.

Figures S3 - S5 below show every run recorded for the binary solutions found to produce intermediate high-pressure hydrate phases. General conclusions about the data shown here do not deviate from those presented in the main text, but we suspect that these additional data may be of interest to researchers studying any one of these solutions in greater depth.
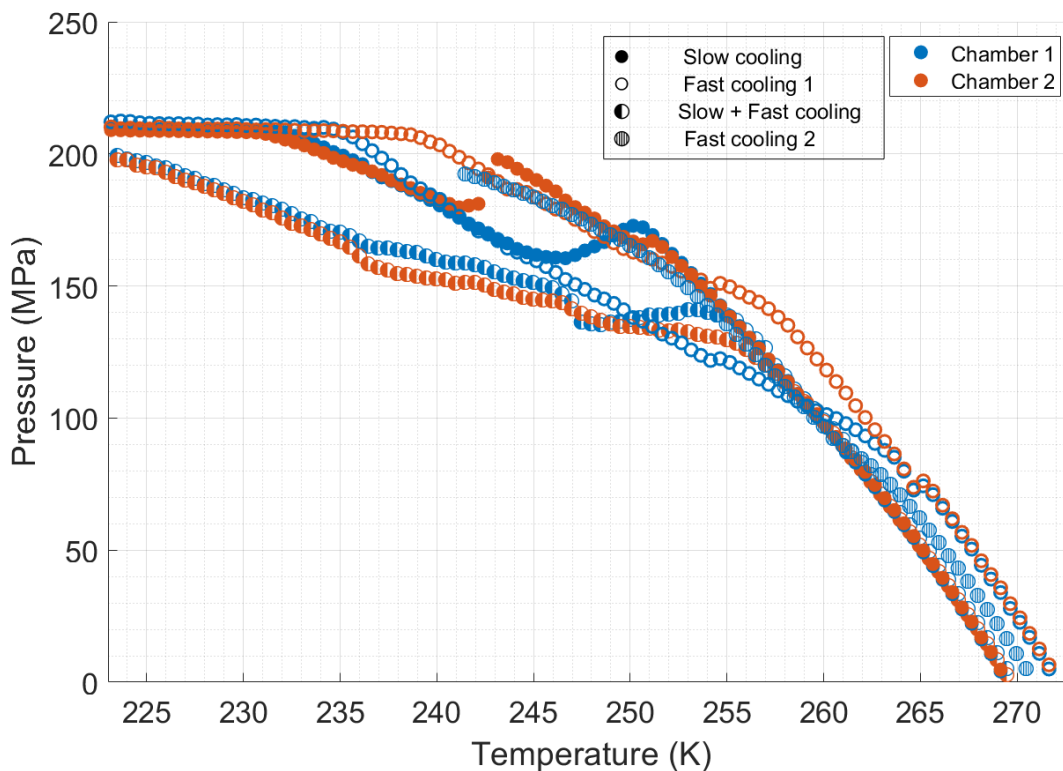

Figure S3. All individual P-T curves recorded for NaHCO3.

NaHCO3 exhibited the greatest diversity of P-T transition features of the solutions considered, and as such, we experimented with additional cooling protocols in an effort to solicit more behaviors. In addition to the slow cooling and slow+fast cooling protocols described in the main text, we also tried two fast cooling protocols:

Fast Cooling 1: Submersion directly from room temperature to 213.15K.

Fast Cooling 2: Submersion directly from room temperature to 241.15K.

In Figure S3 above, it should be noted that the metastable phase configurations and byproducts produced during fast cooling appear to linger to higher temperatures than those for slow cooling. For these protocols, metastable byproducts appear to linger all the way to atmospheric pressure, affecting the recorded atmospheric pressure eutectic point, with greater deviation in eutectic temperature measured for greater cooling rate. While this phenomenon needs significantly more investigation in order to draw any firm conclusions, this behavior suggests that there *may* be metastable hydrates of NaHCO3 that can persist at atmospheric temperature at around 273.15 K. These intermediate phases warrant further investigation, especially via metrological means that may produce more granular information on hydrate structure, such as x-ray diffraction or Raman spectroscopy.
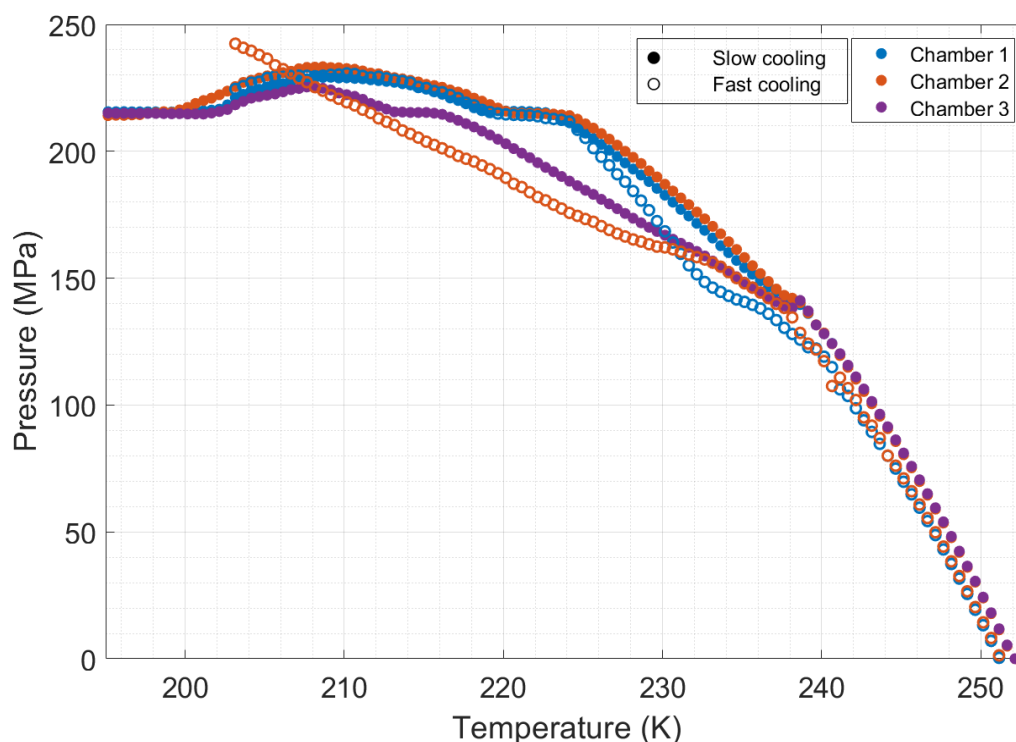
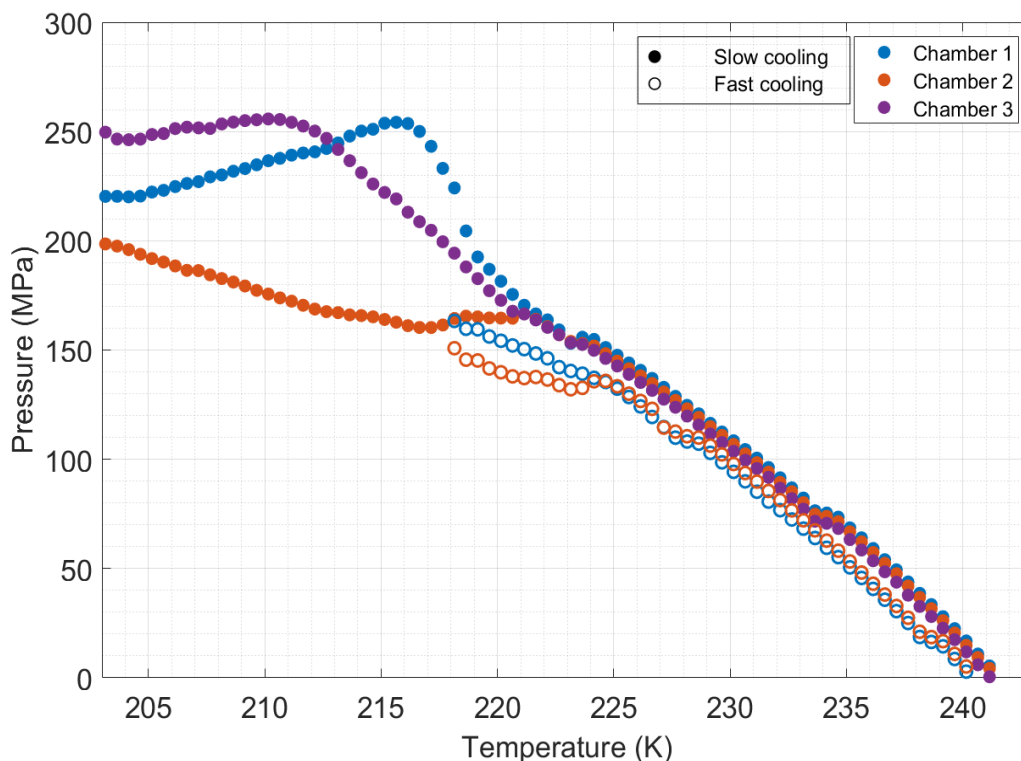Figure S4. All individual P-T curves recorded for NaCl.

Figure S5. All individual P-T curves recorded for MgCl2.

SI References:

1. Pascual, M. R., Trambitas, D., Calvo, E. S., Kramer, H. & Witkamp, G. J. Determination of the eutectic solubility lines of the ternary system NaHCO3-Na2CO3-H2O. *Chemical Engineering Research and Design* **88**, (2010).

2. Li, G., Hwang, Y., Radermacher, R. & Chun, H. H. Review of cold storage materials for subzero applications. *Energy* vol. 51 Preprint at https://doi.org/10.1016/j.energy.2012.12.002 (2013).

3. Pillay, V. *et al.* MgSO4 + H2O system at eutectic conditions and thermodynamic solubility products of MgSO4·12H2O(s) and MgSO4·7H2O(s). *J Chem Eng Data* **50**, (2005).

4. Yuan, L. *et al.* Precise Urea/Water Eutectic Composition by Temperature-Resolved Second Harmonic Generation. *Chem Eng Technol* **39**, (2016).

5. González Díaz, C. *et al.* Thermal conductivity measurements of macroscopic frozen salt ice analogues of Jovian icy moons in support of the planned JUICE mission. *Mon Not R Astron Soc* **510**, (2022).

6. Journaux, B. *et al.* On the identification of hyperhydrated sodium chloride hydrates, stable at icy moon conditions. *Proc Natl Acad Sci U S A* **120**, (2023).

7. Ketcham, S. A., Minsk, L. D., Blackburn, R. R. & Fleege, E. J. Anti-icing: Lower the cost of safer roads. *Public Works* **128**, (1997).